Joint Special Interest Group meeting between euspen and ASPE
Advancing Precision in Additive Manufacturing
KU Leuven, Belgium, September 2023
www.euspen.eu

Center-line-time functions and critical constants for predicting laser powder bed fusion melt pool distortion using one surface topography measurement

Jesse Redford[1,2], Jason Fox[2], Chris Evans[1,2], Brigid Mullany[1], Angela Allen[1], Edward Morse[1]

[1]*Center for Precision Metrology, University of North Carolina at Charlotte, Charlotte, NC, 28223, United States*
[2]*National Institute of Standards and Technology, Gaithersburg, MD, 20899, United States*

tredford@chartlotte.edu

Abstract

This work introduces a center-line-time function (CLTF) to characterize common scan strategies used in laser powder bed fusion (LPBF) that result in melt pool distortion. Eight rapid turnaround (RTR) samples, manufactured from nickel super alloy 625 using a commercial laser powder bed fusion machine with vendor-recommended build parameters, were utilized. The CLTF, in conjunction with a definition of melt pool distortion and a corresponding measurement procedure, was employed to evaluate the length of distorted melt pool regions in these samples. A critical time constant (CTC) was derived from the CLTF and measurement procedure, enabling the prediction of initiation, continuation, and termination locations of melt pool distortion for each sample geometry. Comparing the predicted and measured distorted melt pool lengths, an average error of 0.19 mm ± 0.77 mm was observed, with measured lengths ranging from 1.72 mm to 14.24 mm. The calculated CTC and CLTF values may vary depending on the material and machine parameters used for manufacturing the RTR samples. However, the methodology for determining the CTC and CLTF remains consistent, irrespective of material and machine parameters. These results demonstrate a step towards a quantitative procedure capable of characterizing the occurrence and location of melt pool distortion in both past and future builds. This approach provides practical insights that can aid in understanding and addressing melt pool distortion in laser powder bed fusion processes.

laser powder bed fusion, surface topography, melt pool distortion, swelling, superelevation, critical time constant, process qualification

1. Introduction

Commercial laser powder bed fusion (LPBF) machines often employ fixed process parameters for specific materials, including laser power, scan velocity, and hatch spacing. [1] The vendor-recommended settings offer a general process window for the bulk regions of a build. However, previous studies by [2] have demonstrated that these fixed parameters lead to melt pool distortion in rapid turnaround regions (RTRs), typically found near stripe boundaries or narrow geometric features of the part. This melt pool distortion, resembling swelling [2-5], has been further investigated in recent work [6], which focused on novel part geometries to study the scan strategies and build conditions causing distorted melt pools. The resulting superelevation, where solidified regions exceed the powder layer thickness, poses a risk of impact with the recoater blade during subsequent layer spreading. [7,8] Moreover, variations in the depth of the melt pool, as observed in [6], can introduce irregularities in the subsurface microstructure, impacting both machine health and part quality. Despite the prevalence of distorted melt pool regions in LPBF manufacturing, there remains a need for a quantitative ex-situ procedure to consistently identify and measure these features. By combining prior knowledge of scan strategies and build parameters with reproducible measurements of distorted melt pool regions, it becomes feasible to enhance and evaluate the effectiveness of optimization efforts targeted at eliminating these regions.

2. Methodology

This paper builds upon existing conceptual models [2][6] of distorted melt pool formation in rapid turnaround (RTR) samples. Using coherent scanning interferometry (CSI), we manufactured and measured eight samples with different geometries. To characterize the distorted melt pool regions and laser trajectories used in sample production, we developed a center-line-time function (CLTF) and a corresponding measurement procedure. From these, we derived a critical time constant (CTC) to predict the length of distorted melt pool regions for each sample geometry. By comparing the predicted quantities with manual measurements, we assessed the accuracy of the predictions when utilizing a CTC value based on a distorted melt pool length measurement from a single or multiple RTR samples.

2.1. Rapid Turn-Around Artifacts vs Samples

RTR artifacts, such as the one shown in figure 1, consist of two single layer RTR samples connected by a rectangular waist built on top of a rectangular pedestal. The surface topography of an RTR artifact and a profile section along the center x-axis of the part are shown in figure 1(a) and figure 1(b), respectively. Elevated regions in the build direction caused by distorted melt pools on either end of the sample are shaded in red.

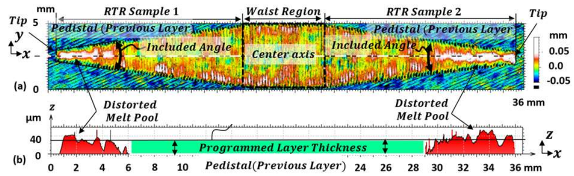

Figure 1. (a) Stitched CSI measurement of manufactured RTR artifact using Zygo Zegage Pro HR with a 5.5× objective showing elevated topography and melt pool distortion at the narrow ends of RTR samples. (b) Profile along the center axis of the artifact showing only isolated regions of elevated topography due to severe melt pool distortion.

The length of a single RTR sample, denoted L_{RTR}, is controlled by a prescribed included angle, expressed as θ_{RTR}. Equation 1 provides a formal expression for the RTR sample length L_{RTR} as a function of the prescribed included angle θ_{RTR}, w, the width of the narrow region, and W, the width of the waist region.

$$L_{RTR}(\theta_{RTR}) = \frac{.5\sin\left(\left(90-\frac{\theta_{RTR}}{2}\right)\right)W}{\cos\left(\left(90-\frac{\theta_{RTR}}{2}\right)\right)} - \underbrace{\left[\frac{.5w}{\tan\left(\frac{\theta_{RTR}}{2}\right)}\right]}_{\Delta x} \qquad (1)$$

The Δx term in equation 1 accounts for the RTR sample trapezoidal geometry. Dimensions of the pedestal upon which the RTR samples and waist region are built are presented in [5].

2.2. Rapid Turn-Around Artifacts and Acquisition Details

A total of eight RTR samples were considered within included angles of 5°, 10°, 15°, 20°, 25°, 30°, and 35°. W was held constant at 5 mm and w held at 1 mm. Each sample is manufactured from nickel super alloy 625 (IN625) using an EOS M290 LPBF machine with vendor-recommended build parameters: laser power of 285 W, scan velocity of 960 mm/s, hatching spacing of 110 µm, and programmed layer thickness of 40 µm. Contouring and stripe boundaries were turned on. The scan strategy is designed such that during the manufacturing of the RTR sample the laser step-over direction is parallel to the x-axis of the RTR sample. The surface topography measurements of the entire sample area were obtained by stitching together multiple individual measurements using Zygo Nexview CSI with a 10× objective and 0.5× tube lens. Data processing was performed in the instrument's native software, using Mx ver. 8.0.0.26, with a 20% stitching overlap. Distorted melt pool regions were isolated, and their lengths were measured following the procedure described in the next section, utilizing MountainsMap™ Version 10.0 software.

2.3. Measurement Procedure for Distorted Melt-Pool Lengths

The following outlines a definition of a distorted melt pool and a procedure for measuring the length of a distorted melt pool in RTR samples, as depicted in figure 2. The purpose of this definition and procedure is to minimize variability in the measurement of the distorted melt pool length by eliminating operator subjectivity in determining the start and end points of the distorted melt pool with respect to the narrow end of an RTR sample. A distorted melt pool is defined as a continuous region of solidified material that exceeds a reference surface. This reference surface is parallel to a best-fit plane through the pedestal region and is offset by the programmed layer thickness (H = 40 µm) along the z-axis. The distorted melt pool length is determined as the maximum perpendicular distance between the narrow end (i.e., tip) of the RTR sample and the end of the distorted melt pool region. By implementing this definition and measurement procedure, the assessment of the distorted melt pool length in RTR samples can be consistently and objectively performed, reducing variability in the measurement process.

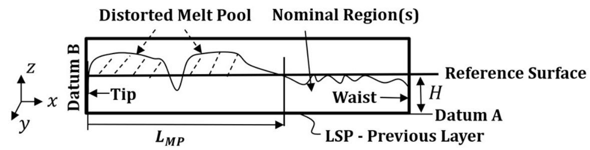

Figure 2. Schematic defining the distorted melt-pool length (L_{MP}). The tip of the RTR geometry is datum B. The end of the distorted melt pool region is the intersection between the surface topography (dashed region) and reference surface offset from a least-squares plane (LSP) through pedestal region (datum A) by the programmed layer thickness (H).

2.4. Derivation of a Center-Line-Time Function and Critical Constants for Predicting Distorted Melt Pool Regions

By leveraging the mirror symmetry about the center x-axis of the RTR artifacts, exemplified in figure 1, a CLTF that characterizes the time needed for the laser to cross the user-defined center-line-axis twice, at any sequential scan increment n, is derived using prior knowledge of the designed laser trajectories, scan velocity (v_s), hatch spacing (Δh), and nominal variables controlling the geometry of the RTR artifact. As shown in figure 3, this is achieved by summing the durations of times t_a, t_b, t_c that describe the three sequential paths the laser must traverse before arriving back at the same nominal position along the center y-axis of the artifact but displaced along the x-axis by a fixed distance, Δh. If the laser begins manufacturing the RTR artifact starting at the left end (i.e., diverging case) it follows that $t_a < t_c$ for each track $n \in \left[0, \frac{L_{RTR_1}}{\Delta h}\right]$, and for the waist region it follows $t_a = t_c$ on the interval $n \in \left[\frac{L_{RTR_1}}{\Delta h}, \frac{L_{RTR_1}}{\Delta h} + \frac{W}{\Delta h}\right]$ until reaching the wide end of the RTR sample on the right (converging case) where $t_a > t_c$ for each sequential track, $n \in \left[\frac{L_{RTR_1}}{\Delta h} + \frac{W}{\Delta h}, \frac{L_{RTR_1}}{\Delta h} + \frac{W}{\Delta h} + \frac{L_{RTR_2}}{\Delta h}\right]$. The skywriting time ($t_b$) where the laser is turned off may vary according to the part geometry and build parameters. Relative to t_a and t_c, small variation in t_b is considered negligible and the average time is assumed constant (i.e., $t_b = \Delta h * v_s^{-1} \in n$). However, further study will be required to measure and quantify the full range and impact of skywriting time variations.

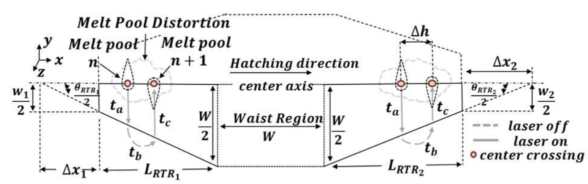

Figure 3. Conceptual illustration of scan strategy used to manufacture RTR samples and examples of diverging (left) and converging (right) cases.

The CLTF for any RTR sample geometry in the case of a diverging scan strategy, depicted in figure 3, is described by equation 2.

$$t(n) = \underbrace{\frac{\tan(\theta_{RTR})\left(\frac{w/2}{\tan(\theta_{RTR}/2)} + \Delta h\, n\right)}{2v_s}}_{t_a} + \underbrace{\frac{\Delta h}{v_s}}_{t_b} + \underbrace{\frac{\tan(\theta_{RTR})\left(\frac{w/2}{\tan(\theta_{RTR}/2)} + \Delta h(n+1)\right)}{2v_s}}_{t_c} \qquad (2)$$

In this equation, $t(n)$ represents the CLTF for the sample and n is a user-defined scan line number that ranges from 0 to $\frac{L_{RTR}}{\Delta h}$. The scan line number acts as an index to track the evolving laser path trajectories along the center axis of the sample. All the variables for calculating the CLTF (e.g., included angle θ_{RTR}, and width w, defining the RTR sample geometry and build parameters including the scan velocity v_s, and hatch spacing Δh) are known or assigned prior to the build. Intuitively, if the duration of time for the laser to cross the center axis of the part twice is less than the time for the melt pool to completely solidify from the previous scan line (i.e., melt pool n shown in figure 3) some amount of melt pool distortion is expected. However, this may be an underestimate of the minimum duration of time to completely avoid melt pool distortion, as the previous statement neglects effects from residual heat in fully solidified material. Still, a conservative assumption regarding the LPBF build process is if any incremental scan strategy trajectory evaluated at an increment n results in a CLTF solution that is less than the time for a nominal melt pool (i.e., quasi-steady state melt pool size in regions free from rapid turnarounds and residual heating effects) to solidify, then some melt pool distortion between adjacent tracks is expected. This is also consistent with the underling mechanisms hypothesized to create the “double wide” weld tracks along stripe boundaries and RTR regions of the build shown in [2]. Calculating a geometry dependent critical constant, n_{crit} , (i.e., the number of scan lines that can be divided into measured length of the RTR sample's distorted melt pool length, L_{MP}) and substituting the value into equation 2, a critical time constant (CTC) value, $t_{crit} = t(n)$, where $n = \frac{L_{MP}}{\Delta h} = n_{crit}$, is acquired and assumed to be independent of the RTR sample geometry. Instead, the calculated value of t_{crit} is a result that characterizes the thermal conditions created by the alloy, machine, and build parameters described in section 2.2. This is because L_{MP} serves as a measurand that encompasses all these factors. By equating the right-hand side of equation 2 to the value of t_{crit} and rearranging the equation to solve for n, we obtain an expression for the track number at which melt pool distortion terminates. Multiplying this non-dimensional expression by the hatch spacing (Δh) yields a closed-form solution to calculate the length of the distorted melt pool in millimeters. This calculation is applicable to samples with various geometries but manufactured with the same build parameters as the RTR sample used to determine t_{crit}. The predicted length of the distorted melt pool (L_{MP}) for any RTR sample geometry, denoted as ($\widehat{L_{MP}}$), is determined using equation 3, which leverages the critical time constant (CTC) value. It represents the distance between the narrow end of an RTR sample (datum B) and the point where the distorted melt pool originates or ends, depending on whether it is converging or diverging. Equation 3 is as follows:

$$\widehat{L_{MP}} = \left(\frac{-0.5\Delta h - \frac{\Delta h}{\tan(\theta_{RTR})} - \Delta x + \frac{t_{crit} * v_S}{\tan(\theta_{RTR})}}{\Delta h} \right) \Delta h \qquad (3)$$

In this equation, Δh, v_s, and t_{crit} are constants, while θ_{RTR} and Δx from equation 1 can be adjusted to predict the length of the distorted melt pool for different RTR sample geometries.

3. Results

3.1. Tabulated Measurements & Critical Constants

Table 1 lists the distorted melt pool length measurements (L_{MP}) for the eight RTR samples using the definition and procedure described in section 2.3. Measurements related to converging cases (i.e., 20º, 25º, 30º, 35º) are shown in white and diverging cases are highlighted as grey rows (i.e., 5º, 10º, 15º, 25º). The critical constants (n_{crit}) were calculated by dividing the measured distorted melt pool lengths (L_{MP}) by the programmed hatch spacing (Δh) of 110 µm. The individual CTC, t_{crit}, values were obtained by evaluating equation 2 according to the calculated n_{crit} and prescribed θ_{RTR} for each sample.

Table 1: Tabulate measurements of distorted melt pool lengths for different RTR sample geometries

Case	θ_{RTR} (º)	L_{RTR} (mm)	L_{MP} (mm)	n_{crit} (no units)	t_{crit} (ms)
Diverging	5	45.81	14.24	129.45	2.46
Diverging	10	22.86	7.91	71.90	2.62
Diverging	15	15.19	5.96	54.18	2.85
Converging	20	11.34	3.13	28.45	2.39
Diverging	25	9.02	3.48	31.63	2.92
Converging	25	9.02	4.07	37.00	3.21
Converging	30	7.46	1.90	17.27	2.41
Converging	35	6.34	1.72	15.63	2.56
$\mu \pm \sigma$					**2.68 ± 0.27**

From table 1, the longest reported distorted melt pool length of 14.24 mm occurs for the 5º included angle and the shortest recorded length of 1.72 mm occurs for the 35º sample (i.e., the widest angle). The distorted melt-pool measurements exhibit an inverse relationship to the included angle of the RTR sample. Comparing the relative ranges of t_{crit} and n_{crit} the variation of the latter is large and dependent on the sample geometry and build parameters, whereas the standard deviation of the former is small and independent of the sample geometry, supporting the assumption that the CTC value, t_{crit}, describes a geometry-agnostic estimate of the minimum duration of time, 2.68 ms ± 0.27 ms in this case, that needs to elapse between sequentially formed melt pools to avoid melt pool distortion when manufacturing IN625 using the machine and build parameters described in section 2.2. A disparity of 0.59 mm is observed between measurements of the diverging and converging cases for the 25° sample geometry that could be related to changes in residual heat effects caused by the laser step-over direction. However, whether this difference exceeds the dispersion of values that can reasonably be attributed to the realization of the measurand (i.e., distorted melt pool length) is yet to be determined. Ongoing work is being conducted to provide a provisional assessment of the Type A and Type B uncertainties associated with the measurement results.

3.2. Predictions vs Measurements for other RTR geometries

The dashed blue line in figure 4 provides a plot of RTR sample length according to a prescribed included angle given by equation 1. Blue text/diamonds correspond to the eight manufactured samples. For example, the manufactured sample with an included angle, θ_{RTR}, of 5º has a length, L_{RTR}, of 45.81 mm. The initiation/end of a distorted melt pool region relative to the narrow end of the sample is indicated with white triangles, Δ and ∇, representing converging and diverging cases, respectively. The vertical distance between a triangle and blue diamond corresponds to the measured distorted melt pool length (L_{MP}) tabulated in table 1. Values are given as black text. The predicted initiation/end regions, according to equation 3, are shown as red crosses (×) with predicted melt pool lengths, $\widehat{L_{MP}}$, given as red text. For example, the measured distorted melt pool length (L_{MP}) for the 5º sample is 14.24 mm and the predicted length ($\widehat{L_{MP}}$) is 15.39 mm. The predicted distorted melt pool lengths given by the dashed red line are based on the CTC value, $t_{crit} = 2.57$ ms, obtained from a single distorted melt pool length (L_{MP}) measurement of 1.72 mm corresponding to the 35º RTR sample. The shaded red regions describe the solution space of predictions if any one of the t_{crit} values shown in table 1 were used as the basis for predicting the distorted melt pool length for all other RTR geometries.

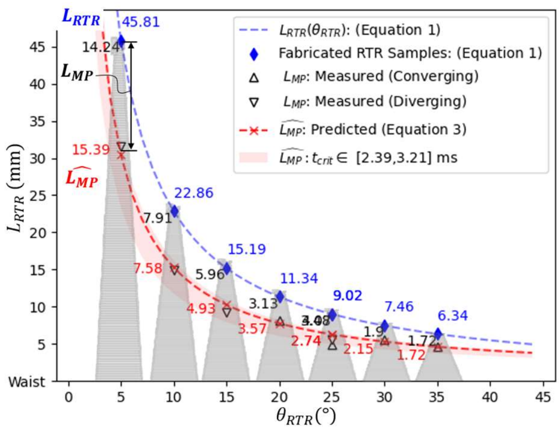

Figure 4. RTR sample length as a function of included angle, 1 mm tip and 5 mm waist, with comparison between the measured versus predicted initiation/end regions and distorted melt pool lengths relative to the tip of the fabricated RTR samples.

Comparing the measurements of distorted melt pool length with the predictions (i.e., $L_{MP} - \widehat{L_{MP}}$) for the eight RTR samples reveals an average error of 0.19 mm with a standard deviation of 0.77 mm. This indicates symmetric errors centered around the mean, with a standard deviation of approximately 7× the hatch spacing. The largest discrepancy of 1.15 mm is observed for the RTR sample with a 5° included angle. Utilizing the average t_{crit} value of 2.68 ms from table 1 results in an average error of -0.22 mm with a standard deviation of 1 mm. Employing the maximum calculated value of 3.21 ms for t_{crit} shifts the predicted trend line to the lower end of the shaded region, while using the minimum value of 2.39 ms shifts the predictions to the upper end. The former CTC value tends to overestimate the distorted melt pool lengths compared to the latter.

4. Summary and Conclusions

A distorted melt pool length measurement of a single RTR sample was used to derive a CTC value that is directly linked to the thermal conditions created by the alloy, machine, and build parameters described in section 2.2. The CTC value is used in conjunction with a CLTF to predict the locations melt pool distortion is expected to initiate, continue, or terminate over a large range of RTR sample geometries. An average error of 0.19 mm ± 0.77 mm was recorded between predicted and measured melt pool lengths, the latter ranging from 1.72 mm to 14.24 mm. The outlined methodology for deriving CLTFs, measuring distorted melt pool lengths, and obtaining a CTC value provides an intuitive approach to characterize why and where melt pool distortion may occur in future or past builds. For example, if manufacturing IN625 using an EOS M290 with vendor recommended settings, the duration of time for the laser to turn around (i.e., skywriting time) at each sequential scan track is consistently less than the range of CTC values obtained using the outlined approach. This implies that the distorted melt pools observed in [2] at stripe boundaries and RTR regions of the build are/can be expected. Increasing the skywriting time to be greater than the calculated CTC value is hypothesized to eliminate melt pool distortion in these areas. The calculated value for this CTC and CLTF may vary depending on the material and machine parameters used to manufacture the RTR samples, but the method of determining the CTC and CLTF is the same regardless of material and machine parameters. The results of this work demonstrate a practical step toward a quantitative procedure that is independent of the specific build, alloy, and machine used. Researchers and manufacturers can utilize this procedure to derive a critical time constant (CTC) value for the characterization, evaluation, and prediction of build parameters and scan strategies that either produce or avoid distorted melt pool regions for different materials. Continuing efforts involve further development, evaluation, and utilization of this CLTF and CTC. Future investigations will explore the links between the calculated CTC and CLTF values with in-situ thermal conditions, as well as melt pool morphology. Additionally, the research will encompass ex-situ measurements of surface topography and subsurface microstructures in both distorted melt pool and nominal regions of RTR samples.

Acknowledgments and Disclaimer

This work was funded by the University of North Carolina at Charlotte's Center for Precision Metrology and the National Institute of Standards and Technology. NIST: J. Tarr (NIST) supported sample fabrication.

Certain commercial entities, equipment, or materials may be identified in this document to describe an experimental procedure or concept adequately. Such identification is not intended to imply recommendation or endorsement by the National Institute of Standards and Technology, nor is it intended to imply that the entities, materials, or equipment are necessarily the best available for the purpose. Contributions of NIST not subject to US Copyright.

References

[1] Yeung, Ho, and Brandon Lane. "A residual heat compensation based scan strategy for powder bed fusion additive manufacturing." Manufacturing letters 25 (2020): 56-59.

[2] Fox, Jason, Christopher Evans, Aarush Sood, Romaine Isaacs, Brigid Mullany, Angela Allen, and Ed Morse. "Weld Track Distortion in Laser Powder Bed Fusion of Nickel Superalloy 625." Proceedings of the ASPE-euspen Special Interest Group Meeting: Advancing Precision in Additive Manufacturing, Knoxville, TN, US, (2022).

[3] Vasileska, Ema, et al. "Layer-wise control of selective laser melting by means of inline melt pool area measurements." Journal of Laser Applications 32.2 (2020).

[4] Sames, William. "Additive manufacturing of Inconel 718 using electron beam melting: processing, post-processing, & mechanical properties." Diss. (2015).

[5] Scime, Luke, et al. "Layer-wise anomaly detection and classification for powder bed additive manufacturing processes: A machine-agnostic algorithm for real-time pixel-wise semantic segmentation." Additive Manufacturing 36 (2020): 101453.

[6] Fox, Jason C., Chris J. Evans, Jordan S. Weaver, and Jesse K. Redford. "Surface Topography and Melt Pool Behavior in Rapid Turnaround Regions of Laser Powder Bed Fusion Additive Manufacturing of Nickel Superalloy 625." CIRP Annals (2023).

[7] Grasso, Marco, et al. "In-process monitoring of selective laser melting: spatial detection of defects via image data analysis." Journal of Manufacturing Science and Engineering 139.5 (2017): 051001.

[8] zur Jacobsmühlen, Joschka, Stefan Kleszczynski, Gerd Witt, and Dorit Merhof. "Elevated region area measurement for quantitative analysis of laser beam melting process stability." In 2015 International Solid Freeform Fabrication Symposium. University of Texas at Austin, (2015).